Fusion Engineering and Design 88 (2013) 2636–2640
DOI:http://dx.doi.org/10.1016/j.fusengdes.2013.05.057

Thermal stability of the grain structure in the W-2V and W-2V-0.5Y_2O_3 alloys produced by hot isostatic pressing

J. Martínez [a], B. Savoini [a], M.A. Monge[a], A. Muñoz [a,*], D.E.J. Armstrong [b], R. Pareja [a]

[a] *Departamento de Física, Universidad Carlos III de Madrid, 28911-Leganés Madrid, Spain*
[b] *Department of Materials, University of Oxford, Park Road, Oxford OX1 3PH, UK*

Highlights:

- W-2V and ODS W-2V-0.5Y_2O_3 alloys have been produced following a powder metallurgy route.
- Grain microstructure and microhardness have been studied after isothermal treatments in vacuum.
- Both alloys exhibit a duplex grain size population: a submicron-sized grain and a coarse grained one.
- The Y_2O_3 addition inhibits growth of the coarse grains for $T < 1973$ K.
- The Y_2O_3 nanoparticles enhance the microhardness of W-2V-0.5Y_2O_3.

Abstract: W-2V and ODS W-2V-0.5Y_2O_3 alloys have been produced following a powder metallurgy route consisting of mechanical alloying and a subsequent high isostatic pressing HIP at 1573 K. The grain microstruc-ture and microhardness recovery of the alloys have been studied in samples subjected to isothermal treatments in vacuum in temperature range 1073–1973 K. Both alloys exhibit a duplex grain size distri-bution consisting of a submicron-sized grain and a coarse-grained population. It has been found that the Y_2O_3 addition inhibits growth of the coarse grains at $T < 1973$ K. Submicron grain growth, with activa-tion enthalpy of 1.9 and 2.49 eV for W-2V and W-2V-0.5Y_2O_3, respectively, was observed at $T \geq 1573$ K. It resulted that the rate constant for grain growth is 30 times higher in W-2V-0.5Y_2O_3 than in W-2V. The considerable enhancement of the microhardness in the W-2V-0.5Y_2O_3 appears to be associated to dispersion strengthening.

Keywords: W alloys, Oxide dispersion strengthened W alloys, Grain growth, Recovery, Microhardness

1. Introduction

Tungsten-base alloys are being considered prime candidate materials for making plasma facing components (PFCs) in the future fusion reactors, in particular for the construction of a He-cooled divertor of the future demonstration fusion reactor (DEMO) [1]. A safe and efficient operating condition of these tungsten PFCs requires new tungsten alloys with enhanced mechanical properties. Solution hardening, dispersion strengthening and grain refine-ment are the traditional approaches applied for developing these tungsten alloys [2–5]. It has been found that the Y_2O_3 addition can induce a relative improvement of the mechanical properties of the W-Ti and W-V alloys, attributable to oxide dispersion strengthen-ing (ODS) and grain refinement induced by the powder metallurgy processing of these alloys [5,6]. In particular, the transmission electron microcopy (TEM) analyses have already established that the oxide dispersion and the grain structure of these ODS W-V alloys have ultrafine characteristics [7]. The mechanical behav-ior of these alloys at high temperature, therefore, will depend on the thermal stability of their microstructure. Although the ultra-fine grained structure is rather unstable it is expected that the dispersion of the stable nanoparticles enhances the microstructure stability by inhibiting the recovery, recrystallization and grain growth. With the aim of evaluating the stability of the ODS nanostructured tungsten alloys, the evolution of the grain microstructure and microhardness recovery of the powder metallurgy W-2V and W-2V-0.5 Y_2O_3 alloys have been studied in samples subjected to isothermal treatments in temperature range 1073–1973 K.

2. Experimental

W-2V and ODS W-2V-0.5Y_2O_3 (wt%) alloys, hereafter referred to as W2V and W2V0.5Y, were produced following a powder metallurgy route consisting of mechanical alloying and subsequent high

* Corresponding author. Tel.: +34 916249413; fax: +34 916248749.
E-mail address: angel.munoz@uc3m.es (A. Mu˜noz).

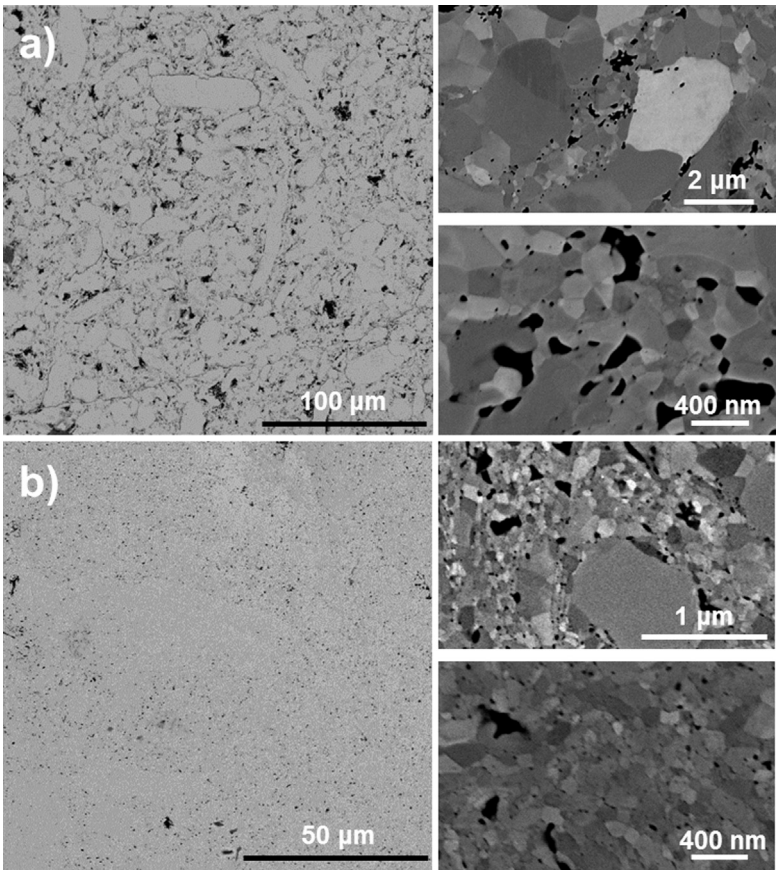

Fig. 1. SEM contrast images showing the structure of duplex grain sizes in (a) W2V y (b) W2V0.5Y. The insets correspond with enlarged ECC images from representatives areas of the low magnification pictures. The black patches in the images consist of pure V in agreement with the energy dispersive analyses.

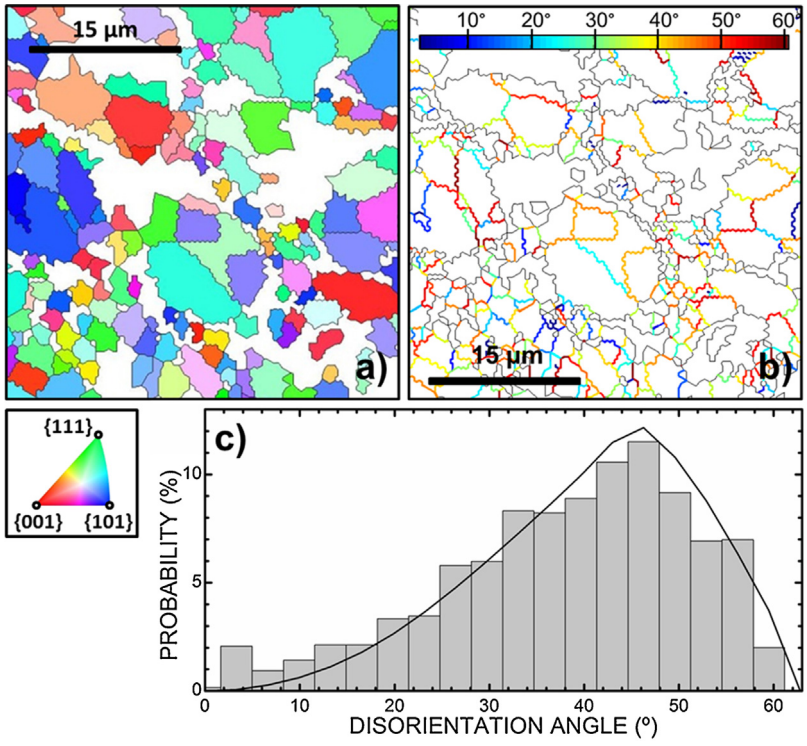

Fig. 2. Quantitative analysis of an EBSD pattern for the W2V alloy: (a) reconstructed EBSD image, (b) boundary disorientation mapping, and (c) boundary disorientation frequency histogram and its theoretical probability density function for an untextured cubic polycrystal. The uncolored patches correspond to grains having sizes below the resolution of the BSE detection system.

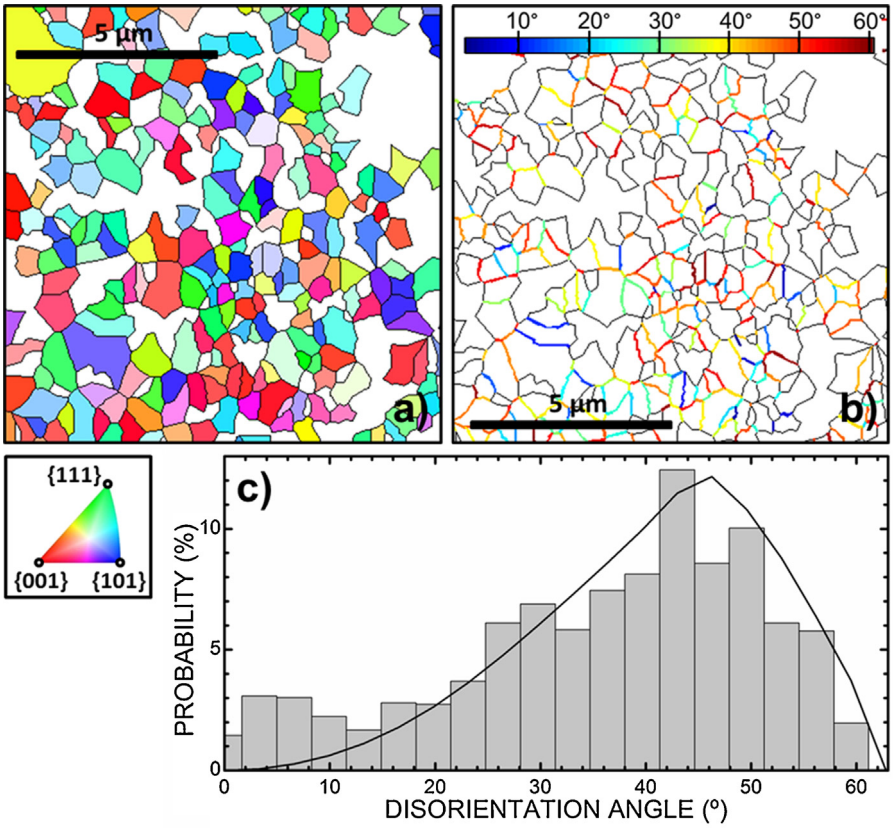

Fig. 3. Quantitative analysis of an EBSD pattern for the W2V0.5Y alloy: (a) reconstructed EBSD image, (b) boundary disorientation mapping, and (c) boundary disorientation frequency histogram and its theoretical probability density function for an untextured cubic polycrystal. The uncolored patches correspond to grains having sizes below the resolution of the BSE detection system.

isostatic pressing (HIP) for 2 h at 1573 K and 200 MPa, following the procedure described elsewhere [8].

Samples of the alloys were vacuum sealed in respective quartz ampoules and subjected to isothermal annealing for 1 h at a given temperature in the range 1073–1973 K, followed by water quenching. After the suitable surface polishing, the microstructure of the samples was examined by electron channeling contrast imaging (ECCI) in a MEB JEOL J8M6500 field emission scanning electron microscope (SEM). In some cases, electron backscatter diffraction (EBSD) patterns from the samples were also acquired using a JSM-6300 scanning electron microscope. The images from the EBSD patterns were reconstructed using the MTex v3.2.5 data analysis software [9]. The applied criterion for discriminating the grain boundaries was a crystallographic misorientation >5° between adjacent crystalline domains.

The experimental distributions of the grain sizes in the samples were determined from the ECC images using an improved approach of the Jhonson–Saltykov stereological method to obtain the spatial grain size distribution of the 3D microstructure from 2D dimensional grain size measurements [10]. Vickers microhardness

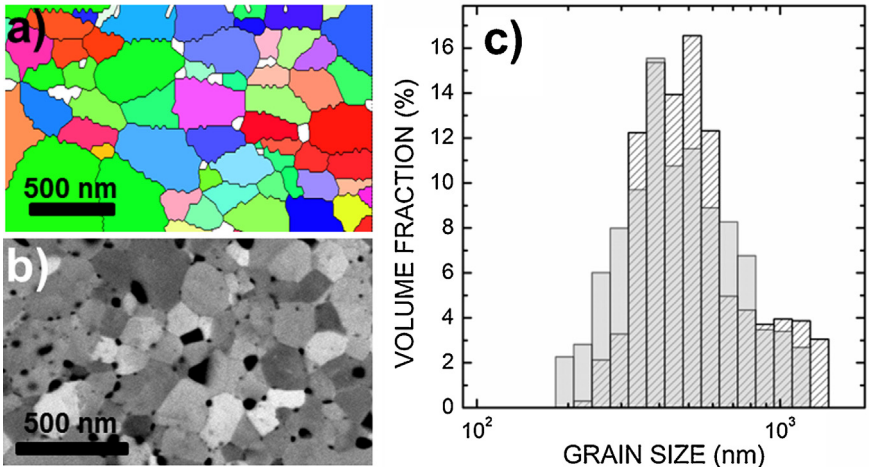

Fig. 4. Grain microstructure of the W2V0.5Y alloy heat treated at 1573 K. (a) reconstructed EBSD image, (b) ECC image and (c) grain size distributions obtained from quantitative analyses from the EBSD (striped bars) and ECC (grey bars) images.

measurements with an applied load of 2.94 N for 20 s were also performed on each specimen.

3. Results and discussion

3.1. Grain microstructure

3.1.1. As-hipped samples

Fig. 1 shows the microstructure of the W2V and W2V0.5Y alloys in the as-HIP condition. The HIP treatment appears to produce V segregation to the powder particles surfaces giving rise to the formation of V pools, which correspond with the black patches revealed by SEM electron channeling images like those shown in Fig. 1. The EDS-SEM analyses of the W2V0.5Y alloys did not reveal the presence of Y_2O_3 indicating that it should be very finely dispersed. The SEM ECC images shown in Fig. 1 reveal that the microstructure of both alloys exhibit intermingled grains having significantly two different sizes, i.e. a duplex grain size distribution comprised of two grain families: one of coarse grains with sizes larger than 1 μm, and a second submicron-sized family. This duplex grain size structure, along with the fact that the ECC images from the coarse grains appear not to show contrast differences attributable to a subgrain substructure, indicate that discontinuous dynamical recrystallization could have occurred during the HIP consolidation. Also, it should be noted that the volumetric fraction of submicron-sized grains in the W2V0.5Y alloy is clearly higher than the fraction of coarse grains, but the opposite occurs in the W2V alloy.

Figs. 2 and 3 show reconstructed EBSD images for the W2V and W2V0.5Y alloys, and the respective quantitative analyses of grain crystallographic orientations along with the corresponding boundary disorientation distributions. Figs. 2b and 3b show the maps of the boundary disorientations, and Figs. 2c and 3c the corresponding frequency histograms along with the Mackenzie boundary disorientation distribution function, which gives the the-oretical probability density of observing a particular boundary disorientation angle in a cubic polycrystalline with their grains randomly oriented, i.e. in an untextured cubic material [11]. Here, the term disorientation corresponds to the lowest angle crystallographically related solution of a misorientation, according to the definition given in Ref. 12. The reasonable agreement of this theoretical distribution with the experimental histograms of boundary disorientation confirms the expected absence of any crystallographic texture in these alloys. Nevertheless, a clear deviation of the experimental frequencies respect to the theoretical ones for disori-entations $\theta < 15^\circ$ is observed for both alloys. This deviation, being more significant in the W2V0.5Y alloy, is attributed to the presence of a high fraction of subgrains, or incidental dislocation boundaries. A fraction of the low-angle boundaries induced by deformation during the mechanical alloying may have resulted in unrecovered subgrains during the HIP consolidation. Also, it appears that the Y_2O_3 addition produces a more recovery resistant alloy by reducing the dislocation mobility, and therefore the subgrain recovery.

3.1.2. Annealed samples

The ECC images did not reveal any significant effect on the grain microstructure of both alloys after annealing at $T \leq 1473$ K, but a vis-ible change in the size distribution of the submicron grains occurred after annealing at 1573 K, as the SEM image shown in Fig. 4, and the size distributions represented in Figs. 5 and 6, reveal. The size distributions represented in Figs. 5 and 6 were determined from quantitative analyses performed on ECC images. In order to vali-date the accuracy of the size distributions determined from the ECC images, the size distribution for the W2V0.5Y heat treated at 1573 K was compared with the one obtained from reconstructed

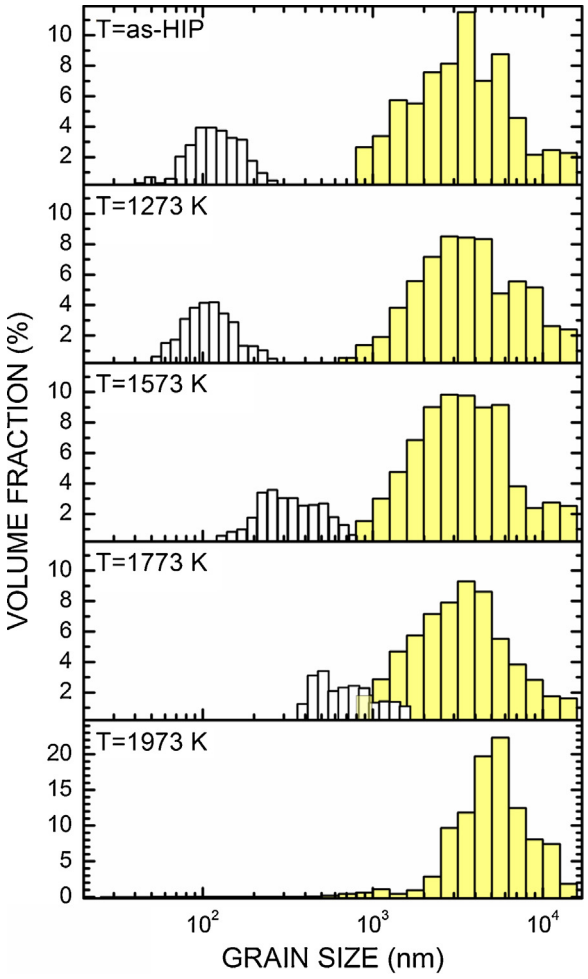

Fig. 5. Duplex grain size distribution for the W2V alloy.

EBSD images. The agreement is very satisfactory as the histograms represented in Fig. 4 reveal considering that the images analyzed correspond to different zones of the sample.

The initial duplex size distribution for both alloys, which are characterized by respective bimodal log-normal distributions, is apparently retained after heat treatments at $T \leq 1473$ K without any perceptible grain growth, as the histograms in Figs. 5 and 6 reveal. The heat treatments at $T \geq 1573$ K induced normal growth of the submicron grains, until the bimodal distributions in both alloys turn into monomodal at 1973 K. It is worthy of notice that: (1) the volume fraction of the submicron grains is significantly higher in W2V0.5Y than in W2V; (2) the volume fraction of the coarse grain population in W2V0.5Y is lower than the corresponding to submicron grains, ~30 against 70%; and (3) the micron-sized grains in W2V0.5Y alloy appear not to coarsen for heat treatments at 1973 K but they do in W2V. The above results confirm that the oxide dispersion inhibits significantly the grain growth of the coarse grains.

According to the classic approach for the kinetics of normal grain growth induced by isothermal treatments, the grain size would be given by [13]:

$$D^2 - D_o^2 = K_o \exp\left(-\frac{Q}{k_B T}\right) t \quad (1)$$

where D_o is the initial size, D the size at time t, Q the activation enthalpy for isothermal growth, T temperature, k_B the Boltzmann constant and K_o a constant. The fits of the experimental data of the submicron-sized grain distributions to Eq. (1) result in an activation enthalpy Q and rate constant K_o for submicron grain growth of

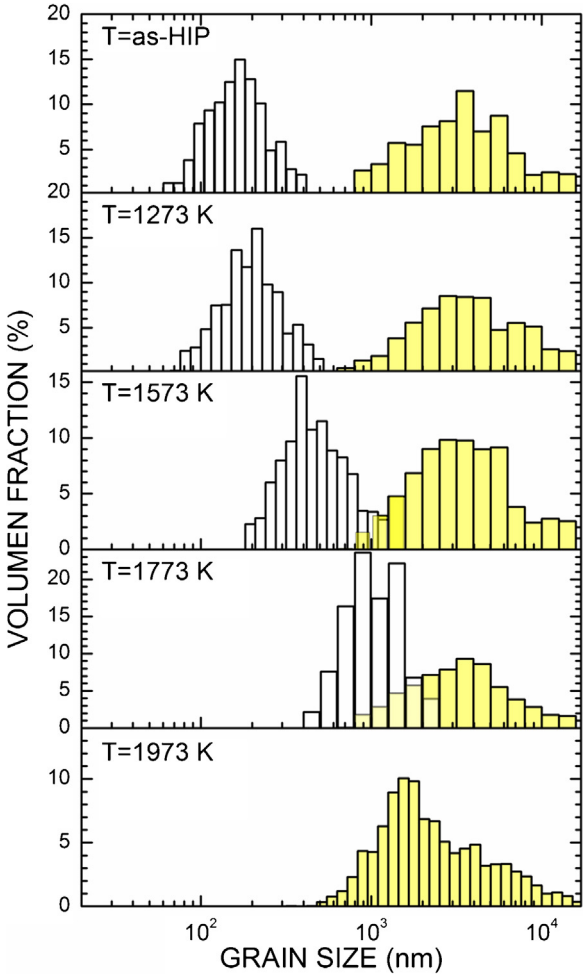

Fig. 6. Duplex grain size distribution for the W2V0.5Y alloy.

1.90 ± 0.06 eV (183 ± 6 kJ/mol) and 4.7×10^{-11} m^2/s for W2V, and 2.49 ± 0.11 eV (240 ± 11 kJ/mol) 1.4×10^{-9} and m^2/s for W2V0.5Y. The activation energy for grain growth is associated to the one for grain boundary diffusion and should be equal to the corresponding activation enthalpy in ideal grain growth. The activation enthalpy values for grain boundary self-diffusion reported for pure tungsten are in the range 377–468 kJ/mol. Moreover, an activation enthalpy for grain growth of 211 ± 13 kJ/mol has been reported for pure tungsten with grain size above 10 μm [14]. The above implies that the submicron-sized grain structure in W2V is quite more unstable that a micron grain structure in pure tungsten. Although the Y_2O_3 addition produces a considerable increase of the activation enthalpy for submicron grain growth, the submicron-sized grain structure is also unstable at 1573 K. However, Y_2O_3 addition inhibits the growth of the coarse grains at 1973 K.

3.2. Microhardness measurements

Fig. 7 shows the effect of the thermal treatments on the microhardness values. The values for W2V0.5Y are between 2.5 and 3 times higher than the corresponding values for W2V. This enhancement appears to be attributable to dispersion strengthening rather than to grain hardening. A recovery onset at ~1573 K is observed for both alloys in coincidence with the submicron grain growth. An unambiguous correlation between the mean grain size of these alloys and the microhardness could not be established.

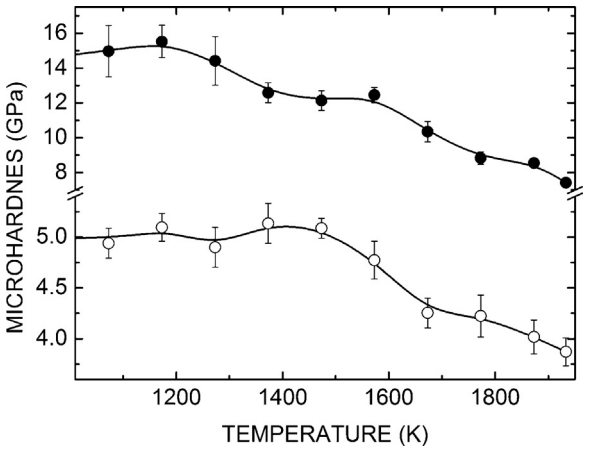

Fig. 7. Microhardness recovery (open circles W2V, closed circles W2V0.5Y).

4. Conclusions

The powder metallurgy W2V and W2V0.5 alloys exhibited a duplex grain size distribution consisting of a submicron-sized grain population and another coarse-grained. It has been found that the Y_2O_3 addition inhibits growth of the coarse grains at $T < 1973$ K, at least. Although the activation enthalpy for submicron grain growth in W2V0.5Y is significantly higher than in W2V alloy, submicron grain growth at 1573 K has been observed in both alloys since the rate constant K_o for W2V0.5Y is higher by a factor of 30. The considerable enhancement of the microhardness in the W2V0.5Y appears to be associated to dispersion strengthening.

Acknowledgments

This work has been supported by the Ministry of Science and Innovation of Spain (MICINN) under contract ENE2012-39787-C06-05, Regional Government of Madrid through the ESTRUMAT-CM program (MAT-1585), and the European Commission through the European Fusion Development Agreement (EFDA). The authors thank to the Microscopy laboratories of the Materials Department (Oxford University) and CENIM (CSIC) for the Electron Microscopy measurements.

References

[1] H. Bolt, V. Barabash, W. Krauss, J. Linke, R. Neu, S. Suzuki, et al., ASDEX upgrade team, Journal of Nuclear Materials 329–333 (2004) 66–73.
[2] M. Schuster, I. Smid, G. Leichtfried, Physica B 234–236 (1997) 1224–1226.
[3] I. Smid, M. Akiba, G. Vieider, L. Plöchl, Journal of Nuclear Materials 258–263 (1998) 160–172.
[4] M.A. Monge, M.A. Auger, T. Leguey, Y. Ortega, L. Bolzono, E. Gordo, et al., Journal of Nuclear Materials 386–388 (2009) 613–617.
[5] M.V. Aguirre, A. Martín, J.Y. Pastor, J. Llorca, M.A. Monge, R. Pareja, Journal of Nuclear Materials 404 (2010) 203–209.
[6] A. Mu˜noz, J.Y. Pastor, R. Pareja, M.A. Monge, B Savoi, T. Leguey, et al., 1st Monitoring Meeting of MAT-W&W Alloys Project, in: EFDA, Garching, Germany, 7–9th February 2012, 2012.
[7] J. Martínez, B. Savoini, M.A. Monge, A. Mu˜noz, R. Pareja, Fusion Engineering and Design 86 (2011) 2534–2537.
[8] A. Mu˜noz, M.A. Monge, B. Savoini, M.E. Rabanal, G. Garcés, R. Pareja, Journal of Nuclear Materials 417 (2011) 508–511.
[9] F. Bachmann, R. Hielscher, H. Schaeben, Ultramicroscopy 111 (2011) 1720–1733.
[10] Y.H. Xu, H.C. Pitot, Computer Methods and Programs in Biomedicine 72 (2003) 1–20.
[11] J.K. Mason, C.A. Schuh, Acta Materialia 57 (2009) 4186–4197.
[12] V. Randle, O. Engler, Introduction to Texture Analysis, Gordon and Breach Science Publishers, 2000, pp. XIV.
[13] H. Gleiter, Acta Metallurgica 48 (2000) 1–29.
[14] J. Almanstötter, M. Rühle, International Journal of Refractory Metals and Hard Materials 15 (1997) 295–300.